Unraveling Reaction Path Bifurcation: Insights into Electron Movement via Natural Reaction Orbitals

Tatsuhiro Nakanishi,[a] Takuro Tsutsumi,[b] Yuriko Ono,[c] Kazuki Sada,[b] and Tetsuya Taketsugu[b,c*]

[a] *Graduate School of Chemical Sciences and Engineering, Hokkaido University, Sapporo 060-0810, Japan*
[b] *Department of Chemistry, Faculty of Science, Hokkaido University, Sapporo 060-0810, Japan*
[c] *Institute for Chemical Reaction Design and Discovery (WPI-ICReDD), Hokkaido University, Sapporo 001-0021, Japan*

Abstract

This study investigates the Beckmann rearrangement of 1-phenyl-2-propanone oxime derivatives, focusing on the reaction path bifurcation behavior from the perspective of electron movement. The previous work reported that electron-withdrawing substituents drove the reaction toward the rearrangement pathway, while electron-donating substituents favored the fragmentation pathway. Through Natural Reaction Orbital (NRO) analysis, this research demonstrates how electrons move at critical branching points, specifically in the directions of the intrinsic reaction coordinate (IRC) and the projected vibrational mode associated with the branching behavior. The NRO approach, which complements traditional IRC and *ab initio* molecular dynamics methods, not only provides valuable quantitative insights for predicting product distributions but also aids in the strategic design of substituents for desired products. These findings extend our understanding of reaction mechanisms and byproduct formation, offering fresh perspectives on complex chemical transformations.

Keywords: natural reaction orbital, bifurcation, Beckmann rearrangement, substituent effect

*Corresponding authors: Tetsuya Taketsugu (take@sci.hokudai.ac.jp)

1. Introduction

The Born-Oppenheimer approximation separates the treatment of electronic states and nuclear motion and introduces the potential energy surface (PES) with atomic coordinates as variables. On the PES, reactants and products correspond to minimum points, while the transition state (TS) is defined as a first-order saddle point. To describe the elementary chemical reaction process, Fukui introduced the intrinsic reaction coordinate (IRC), which is defined as the minimum energy path that connects the reactants, TS, and products in mass-weighted coordinates [1,2]. The IRC preserves molecular structural symmetry at non-stationary points because the energy gradient vector belongs to the totally symmetric representation [3]. In relation to this symmetry principle, it was discovered that a phenomenon called valley-ridge inflection (VRI) can occur in certain vibrational modes orthogonal to the IRC [4]. In such cases, the frequency of non-totally symmetric modes that break geometric symmetry changes from real to imaginary along the IRC, causing the PES shape to shift from a valley to a ridge. If this ridge-like shape persists until the end of the IRC, the IRC terminates at a second TS, which then branches into two products with reduced symmetry. The concept of VRI has been discussed in relation to reaction path bifurcations [4-7]. One of the authors clarified that VRI occurs in regions where the vibronic interaction between the electronic ground state and excited states along the IRC becomes significant, based on the second-order Jahn-Teller theory [8]. Such instability of the IRC also arises along totally symmetric vibrational modes orthogonal to the IRC, which are eigenfunctions of the projected Hessian matrix [9]. This phenomenon is known as a valley-ridge transition (VRT) [10]. VRTs have been observed along IRC paths in many organic reactions, leading to

branching into different types of products [11]. These findings highlight that standard IRC calculation may overlook certain reaction products [12]. Currently, reaction path bifurcation is being recognized as a crucial factor in various organic and enzymatic reactions [13-15].

The IRC pathway is determined by the shape of the PES, which, in principle, is governed by the electronic wavefunction. Among the various reactivity theories that focus on electronic wavefunctions in elementary reaction processes, the frontier molecular orbital theory, based on the highest-occupied molecular orbital (HOMO) and lowest unoccupied molecular orbital (LUMO), is well-known [16]. This widely applicable theory suggests that a chemical reaction occurs when the most active electron interacts with the most stable vacancy, leading to electron delocalization and stabilization. According to this theory, if the HOMO and LUMO of the reactants overlap effectively and in-phase, the reaction is more likely to proceed. However, advances in automated reaction path search methods [2,17] have revealed that understanding complex chemical reaction processes requires considering a reaction path network composed of multiple IRCs rather than a single IRC. In such cases, focusing solely on HOMO and LUMO associated with a single elementary reaction process is insufficient for accurately predicting chemical reactions. Recently, Tsuneda *et al*. developed the reactive orbital energy theory (ROET) [18], which is based on Kohn-Sham orbitals obtained from long-range corrected density functional theory (LC-DFT) calculations. ROET determines reactive occupied and virtual orbitals by tracing orbital energy changes along the IRC [19]. ROET was applied to 37 different IRCs derived from the glycine structure, and it was found that each IRC corresponds to a unique pair of reactive orbitals, emphasizing the diverse electronic nature of reaction pathways [20].

In recent years, we have developed a new method called the Natural Reaction Orbital (NRO) method [21], which visualizes changes in electronic wavefunctions along reaction pathways as pairs of occupied and virtual orbitals. The NRO method was initially formulated for single-configuration-based methods, such as the Hartree-Fock and DFT methods, and was later extended to a multi-configuration wavefunction theory [22]. Using the NRO method, we have successfully revealed the behavior of electron motion along IRCs for various types of chemical reactions [21,22].

In this study, we apply the NRO method to reactions exhibiting bifurcation to investigate the branching mechanisms from an electron movement perspective. As a demonstration, we selected the Beckmann rearrangement of 1-phenyl-2-propanone oxime derivatives, a reaction in which Yamataka *et al.* identified the presence of reaction path bifurcations occurring after the TS [23,24]. This post-transition state bifurcation leads to either a rearrangement or fragmentation product due to the bifurcation of the reaction path (**Fig. 1**). We will also focus on substituent effects that influence the branching behavior.

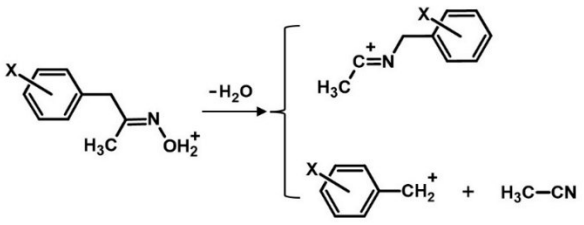

Figure 1. Reaction bifurcation scheme of the Beckmann rearrangement (top) and fragmentation (bottom) pathways.

2. Methodology

The NRO method analyzes changes in electronic wavefunctions along the IRC by extracting orbital changes [21] rather than tracking orbitals themselves. In this sense, it fundamentally differs from methods such as ROET [18-20], which selects and tracks reactive orbitals among canonical orbitals along the IRC, and the IBO method [25, 26], which tracks localized orbitals along the IRC. The NRO method unveils electronic structure changes by precisely analyzing the derivative of molecular orbitals with respect to nuclear coordinates [21]. For a given molecular structure, if an arbitrary nuclear displacement is represented as τ, the resulting change in molecular orbitals can be expressed as:

$$\mathbf{C}(\tau) = \mathbf{C}(0) + \tau\left(\mathbf{C}(0)\mathbf{U}^{(1)}(0)\right) \tag{1}$$

where $\mathbf{C}$ is the molecular orbital coefficient matrix, 0 represents the structure before displacement, and $\mathbf{U}^{(1)}(0)$ is the matrix of the derivatives of molecular orbital coefficients with respect to nuclear coordinates, obtained as a solution to the coupled-perturbed SCF (CP-SCF) equations [27-30]. The occupied-virtual component of $\mathbf{U}^{(1)}$, $\mathbf{U}^{(1)}_{\mathbf{VO}}$, describes mixing of occupied and virtual orbitals induced by nuclear displacements, indicating changes in bond order or electron movement. To obtain a good basis for $\mathbf{U}^{(1)}_{\mathbf{VO}}$, singular value decomposition (SVD) is performed:

$$\mathbf{U}^{(1)}_{\mathbf{VO}} = \mathbf{V}\boldsymbol{\Lambda}\mathbf{O}^{\dagger} \tag{2}$$

where $\boldsymbol{\Lambda}$ is a rectangular diagonal matrix of size $N_{vir} \times N_{\mathrm{occ}}$ (N_{vir} is the number of virtual orbitals, and N_{occ} is the number of occupied orbitals, generally $N_{vir} > N_{\mathrm{occ}}$), which contains singular values λ_i, represented as:

$$(\boldsymbol{\Lambda})_{ij} = \lambda_j \delta_{ij} \;\; (1 \le i \le N_{vir}, 1 \le j \le N_{\mathrm{occ}}) \tag{3}$$

The non-zero singular values λ_i quantify the extent of orbital mixing. By sorting the column vectors of the unitary matrices $\mathbf{O}$ and $\mathbf{V}$ in descending order of λ_i, and transforming the molecular orbital coefficient matrix $\mathbf{C}$ using $\mathbf{V}$ for virtual orbitals and $\mathbf{O}$ for occupied orbitals, we obtain the NRO coefficients $\boldsymbol{n}$:

$$\left(\boldsymbol{n}_1, \cdots, \boldsymbol{n}_{N_{\mathrm{occ}}}\right) = \left(\boldsymbol{c}_1, \cdots, \boldsymbol{c}_{N_{\mathrm{occ}}}\right)\mathbf{O} \tag{4.1}$$

$$\left(\boldsymbol{n}'_1, \cdots, \boldsymbol{n}'_{N_{\mathrm{vir}}}\right) = \left(\boldsymbol{c}_{N_{\mathrm{occ}}+1}, \cdots, \boldsymbol{c}_{N_{\mathrm{occ}}+N_{\mathrm{vir}}}\right)\mathbf{V} \tag{4.2}$$

where $\boldsymbol{c}_i$ represents the coefficient vector of the i-th molecular orbital, and $\boldsymbol{n}_i$ ($\boldsymbol{n}'_i$) represents the coefficient vector of the i-th NRO ϕ_i (ϕ'_i). The change in NROs due to nuclear displacement is expressed as:

$$\phi_i(0) \rightarrow \phi_i(0) + \tau\lambda_i\phi'_i(0)\ (i = 1,2, \cdots N_{\mathrm{occ}}) \tag{5}$$

Eq. (5) indicates that the mixing of occupied and virtual NROs represents the change in NROs. The degree of mixing is determined by the singular value λ_i, which quantifies the extent of electron movement associated with orbital mixing. The sum of the squared singular values, which is mathematically equal to the squared Frobenius norm of $\mathbf{\Lambda}$, serves as an indicator of the overall extent of orbital mixing for a given nuclear displacement:

$$\sum_{i=1}^{N_{occ}} \lambda_i^2 = \|\mathbf{\Lambda}\|_F{}^2 \tag{6}$$

Additionally, the density change due to nuclear displacement can be expressed as:

$$\rho^{(1)} = \sum_{i=1}^{N_{occ}} \lambda_i(\phi_i'^*\phi_i + \phi'_i\phi_i^*) \tag{7}$$

By conducting NRO analysis at each point along the reaction path, we can track the changes in NRO shape and $\|\mathbf{\Lambda}\|_F{}^2$ values along the path. Larger $\|\mathbf{\Lambda}\|_F{}^2$ values indicate significant

electron movement due to mixing between occupied and virtual orbitals. These values help identify the important regions for electron movement along the reaction path. Typically, $\|\mathbf{\Lambda}\|_F{}^2$ value is larger in regions where TS is close by or where bonding nature changes. By focusing on the density changes given by Eq. (7), we can identify the primary electron movement events from the contributions of NRO pairs with large singular values.

There are several types of research to analyze chemical properties and reactions by applying SVD to the **U** matrix. The first example is the discussion of solvent effects by Morita *et al.* [31]. The Natural Perturbation Orbital (NPO) method also applies SVD to the **U** matrix in order to elucidate the mixing between occupied and virtual orbital spaces by certain perturbation, which has been used to analyze factors contributing to changes in Raman intensity when an electric field is applied [32,33]. Recently, the Natural Transition Orbital (NTO) method has gained widespread use in calculations of electronic excited states using the time-dependent DFT method. By applying SVD to the elements of the transition density matrix, the NTO method extracts pairs of occupied and virtual orbitals that characterize electronic transitions for the target excited state [34]. Thus, the extraction of orbital pairs using SVD can provide insights into electronic structure changes under various perturbations, including structural deformations, electric fields, and electronic excitations.

In this study, we apply the NRO method to investigate the problem of reaction path bifurcation. First, NRO analysis is performed along the IRC to elucidate the behavior of electron movement associated with structural changes along the reaction coordinate. Subsequently, vibrational analysis along the IRC is conducted to identify the VRT points. In these regions, vibrational modes orthogonal to the IRC (projected vibrational modes) are

analyzed to determine the branching direction. It should be noted that the fluctuations observed in the orthogonal frequencies in the following sections are attributed to instabilities in the relative orientations and potential energy gradients associated with the dissociation of the water molecule. These fluctuations were reproduced even when more precise IRC calculations were performed. The NROs associated with structural displacements along this branching direction are then extracted. By examining electron movement behavior along the two diverging pathways in the bifurcation region, we aim to clarify the nature of branching reactions from the perspective of electron movement. This approach should provide a detailed understanding of the electronic behavior underlying reaction path bifurcations, contributing to a more comprehensive picture of complex chemical reaction dynamics.

3. Computational details

The reaction path analysis of bifurcation reactions of 1-phenyl-2-propanone oxime derivatives (X = *p*-NH_2, *p*-OMe, *m,m'*-Me_2, *p*-Me, *m*-Me, H, *p*-Cl, *p*-CHO, *p*-CN, *p*-NO_2) was conducted at the ωB97X/6-31G* level. Depending on the substituent X, the IRC pathways for these derivatives exhibit either a Beckmann rearrangement or fragmentation [23,24]. First, the TS structures were located, and then IRC calculations were performed to confirm which product the IRC pathway led to. Additionally, projected vibrational modes were computed along the IRC to check for VRT points. Subsequently, NRO analysis was performed along the IRC. Normal mode analysis was conducted for each structure along the IRC to obtain the **U** matrix, using the keyword IOp(10/21=1) to extract the **U** matrix as a solution of the CP-SCF equations. SVD was employed for the **U** matrix components, allowing the NRO along the IRC to be determined. To investigate the behavior of NRO at reaction path bifurcation points, the projected vibrational mode corresponding to the bifurcation direction was selected, and the NRO associated with the branching direction was computed. All electronic structure calculations were performed using Gaussian16 Rev.C.01 [35].

4. Results and Discussion

A. IRCs for the Beckmann rearrangement of 1-phenyl-2-propanone oxime derivatives

First, TS structures were explored, and IRC calculations were performed for the Beckmann rearrangement of 1-phenyl-2-propanone oxime derivatives (X = *p*-NH_2, *p*-OMe, *m,m'*-Me_2, *p*-Me, *m*-Me, H, *p*-Cl, *p*-CHO, *p*-CN, *p*-NO_2). The results are shown in **Fig. 2**, where the horizontal axis represents the reaction coordinate, *s*, and the vertical axis indicates the atomic distance between the benzylic carbon and the nitrogen, distinguishing rearrangement from fragmentation paths. Among the ten substituents, eight exhibited rearrangement reactions, whereas the highly electron-donating substituents *p*-NH_2 and *p*-OMe led to fragmentation products. This trend aligns with previous studies conducted at the MP2 level [23,24].

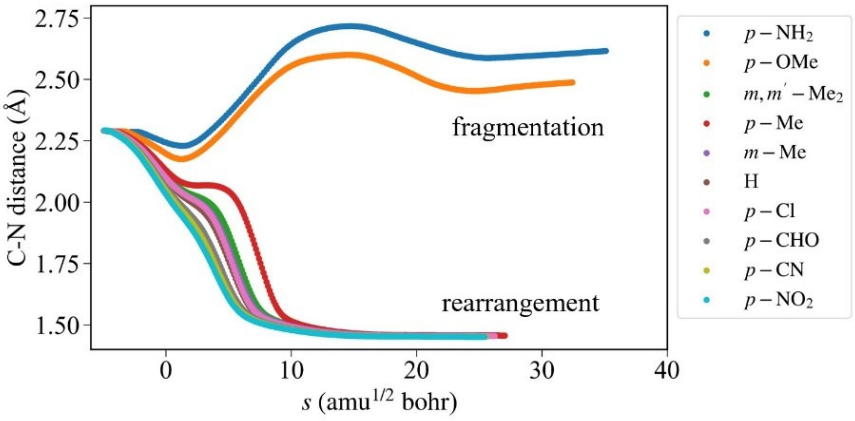

Figure 2. Changes in the C-N distance along the IRC for the Beckmann rearrangement or fragmentation of 1-phenyl-2-propanone oxime derivatives (X = *p*-NH_2, *p*-OMe, *m,m'*-Me_2, *p*-Me, *m*-Me, H, *p*-Cl, *p*-CHO, *p*-CN, *p*-NO_2).

B. NRO Analysis of the Beckmann Rearrangement for X = H

This section discusses the results of NRO analysis along the IRC for the Beckmann rearrangement of the unsubstituted compound (X = H). **Figure 3a** shows the structures of the reactant, TS, and product connected along the IRC. These structural changes indicate that the dissociation of a water molecule occurs before reaching the TS, and then the rearrangement reaction completes as proceeding from the TS to the product. Figure 3b illustrates the energy profile (black) and the changes in $\|\mathbf{\Lambda}\|_F^2$ (red) obtained from the NRO analysis (Eq. (6)) along the IRC. $\|\mathbf{\Lambda}\|_F^2$ corresponds to the squared Frobenius norm of $\mathbf{U}_{\mathbf{VO}}^{(1)}$, where larger values indicate a greater degree of orbital mixing. While the energy profile shows a maximum at the TS, the NRO analysis reveals distinctive features: the changes in $\|\mathbf{\Lambda}\|_F^2$ show shoulder-like behavior at $s = -3.31$ amu$^{1/2}$ bohr and peaks at $s = 0.35$ and 4.96 amu$^{1/2}$ bohr. These peaks correspond to regions where significant electron movement and bond changes occur. In general, reactions in which multiple bond changes occur within a single elementary reaction are interpreted as concerted reactions. However, the NRO analysis has revealed that even in reactions generally considered to be concerted, multiple bond change processes can occur sequentially.

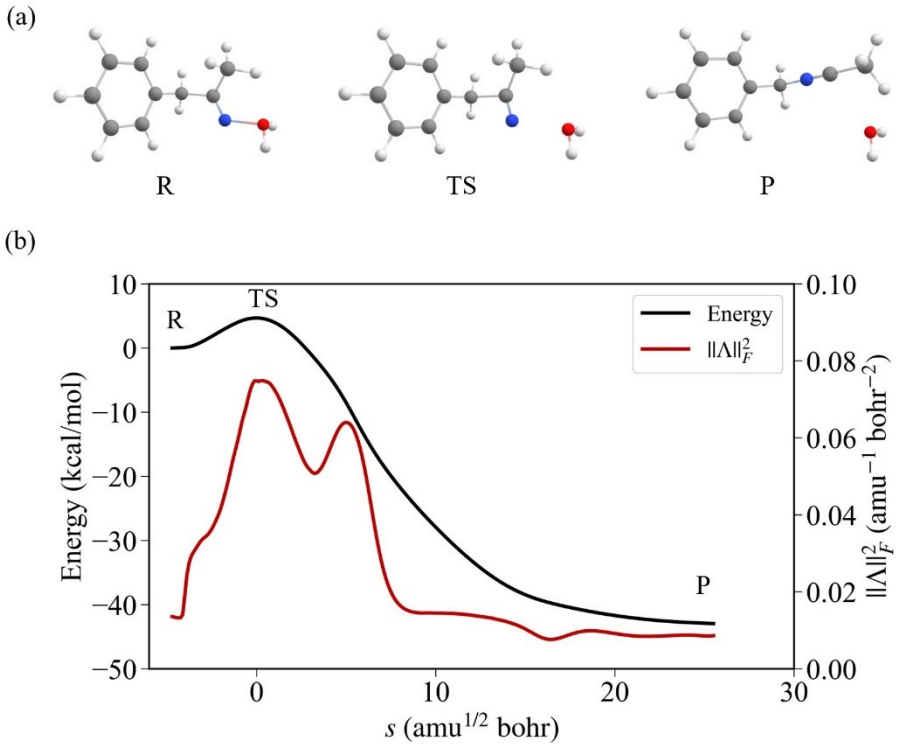

Figure 3. The Beckmann rearrangement reaction for the unsubstituted compound (X = H): (a) Structures of the reactant (R), TS, and product (P). (b) Changes in energy (black) and $\|\boldsymbol{\Lambda}\|_F^2$ (red) along the IRC.

The nature of electron movement at each peak can be understood by examining the corresponding NROs. **Figure 4** shows the most significant occupied NRO ϕ_1, virtual NRO ϕ_1', and their product $\phi_1\phi_1'$ obtained at the pre-TS, TS, and post-TS peaks. In NRO analysis, structural changes along the reaction coordinate are interpreted as inducing mixing between the occupied and virtual NROs. By multiplying these orbitals, it becomes possible to visualize how the electron moves during the structural transformation (Eq. (7)). The cyan regions represent areas where electron density decreases due to the mixing of orbitals with

opposite phases, while the yellow regions indicate areas where electron density increases due to the mixing of orbitals with the same phase. Therefore, the electron moves from the cyan regions to the yellow regions. To the right of each NRO pair, the corresponding singular value and the contribution ratio of the NRO pair, defined by the following, are provided.

$$\frac{\lambda_i^2}{\sum_j \lambda_j^2} \tag{8}$$

In other words, although multiple NRO pairs are defined for each structure, electron movement should be discussed by focusing on the NRO pairs with large singular values and high contribution ratios. The contribution ratios of the NRO pairs shown in Fig. 4 range from 67% to 75%, indicating relatively high values. This confirms that the electron movement at each peak can be effectively discussed based on these NRO pairs.

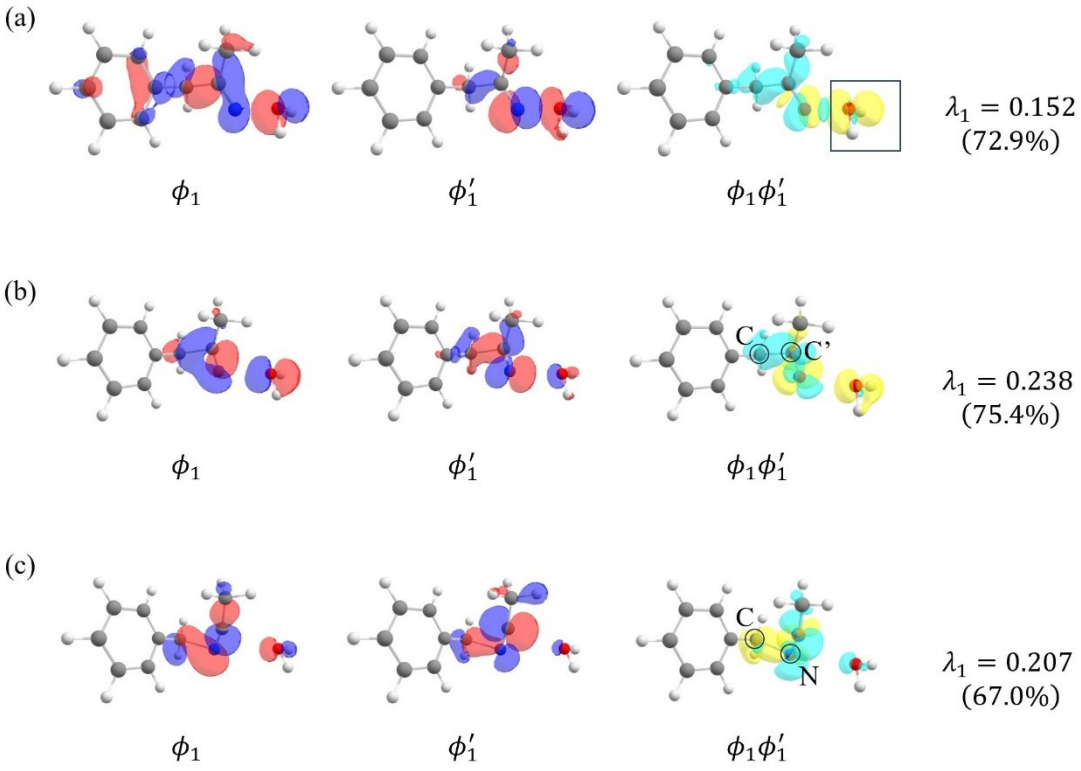

Figure 4. Occupied NRO (ϕ_1), virtual NRO (ϕ_1'), and their product ($\phi_1\phi_1'$) at the $\|\mathbf{\Lambda}\|_F^2$ peaks for the unsubstituted compound (X = H): (a) $s = -3.31$ amu$^{1/2}$ bohr, (b) $s = 0.35$ amu$^{1/2}$ bohr, and (c) $s = 4.96$ amu$^{1/2}$ bohr.

Fig. 4a shows the NROs at the initial peak of $\|\mathbf{\Lambda}\|_F^2$ where the water molecule dissociates. In this Beckmann rearrangement, as H_2O dissociates, the H_2O moiety changes from a monovalent cation to a neutral state (indicated by the natural population analysis [36] along the IRC, as shown in Supporting Information (SI), Fig. S1-1). This process is accompanied by electron movement from the cyan to the yellow regions within the molecule, illustrating electron movement to H_2O. Fig. 4b illustrates electron movement near the TS. While qualitatively similar to Fig. 4a, a notable feature is the significant decrease in electron

density of the C-C' σ orbital, suggesting bond dissociation. Fig. 4c shows electron movement to the C-N σ orbital, which characterizes the rearrangement reaction.

These observations demonstrate that NRO analysis can automatically extract multiple bond changes and associated electron movement events in the Beckmann rearrangement. Even when a single elementary reaction involves multiple bond changes, NRO analysis enables automatic extraction of the electron movement associated with each bond change at the orbital level. The ability to automatically identify both the "regions where bond changes occur" and the "orbital pairs driving the bond changes" enhances our understanding of reaction mechanisms, highlighting the effectiveness of the NRO method.

Next, we move to the analysis of reaction path bifurcations. First, projected vibrational modes were calculated along the IRC, and their frequencies were plotted, as shown in **Fig. 5a**. The frequencies change from real to imaginary values as the PES changes from a valley to a ridge in the direction orthogonal to the IRC. Among several imaginary frequencies observed, one particular mode - shown in blue - rapidly decreases after crossing the TS. Figure 5b illustrates the vibrational mode corresponding to this imaginary frequency. This mode represents the dissociation behavior of the two fragments, the benzyl cation and CH_3CN, and clearly captures the molecular motions associated with the fragmentation process of interest in this study. Therefore, we selected this mode as the key projected vibrational mode that drives the VRT in the bifurcation direction. It is important to note that other modes with imaginary frequencies correspond to structural changes such as the internal rotation of the H_2O moiety, which are not directly relevant to the reaction under investigation.

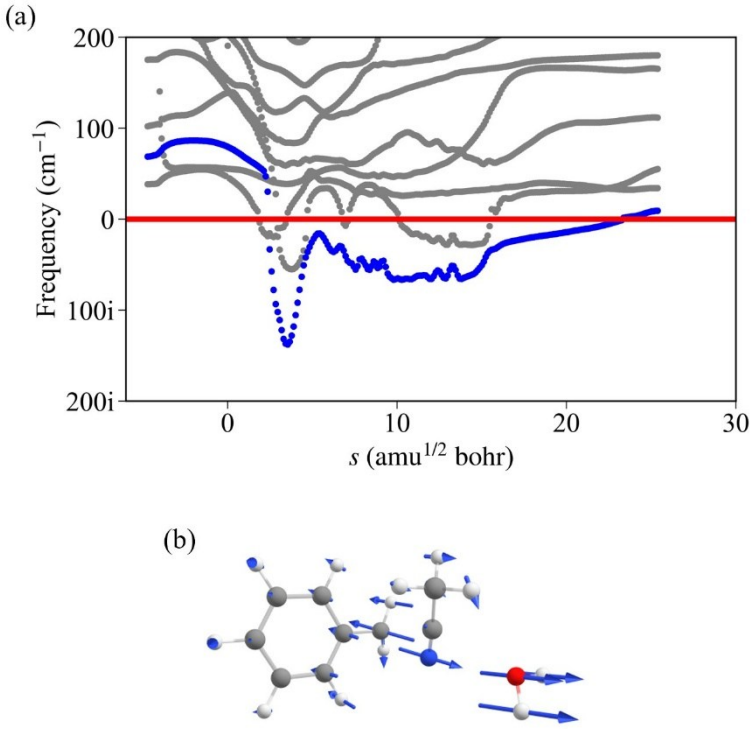

Figure 5. (a) Changes in the frequencies of projected vibrational modes along the IRC for the Beckmann rearrangement of the unsubstituted compound (X = H), where the blue line represents the frequency of the vibrational mode leading to fragmentation. (b) The projected vibrational mode corresponding to fragmentation.

NRO analysis can also analyze electron movement for arbitrary structural changes. Here, in the ridge region of the IRC following the VRT, electron movement was analyzed using NRO for two types of structural changes: one along the IRC direction and the other along the branching direction, corresponding to the projected vibrational mode that leads to the branching product. The branching direction mode was taken as the one shown in Fig. 5b, and NRO analysis was performed at $s = 3.54$ amu$^{1/2}$ bohr, where the imaginary number of the frequency is maximized. This result is shown in **Fig. 6**. The NRO results along the IRC direction (Fig. 6a) are nearly identical to those in Fig. 4c, indicating electron movement from CH_3CN to the C-N σ orbital, leading to the formation of the C-N bond. In contrast, structural changes in the branching direction (Fig. 6b) show electron movement from the benzene ring toward CH_3CN. Before reaching the branching point, CH_3CN is positively charged due to the dissociation of H_2O (see Fig. S1-1), but as fragmentation proceeds, the electron moves from the benzene side to the CH_3CN side, allowing CH_3CN to dissociate as a neutral fragment (see Fig. S1-2, which shows the change of natural charge in case of fragmentation reaction). NRO analysis successfully visualized the electron movement driving the bifurcation, providing deeper insight into the reaction mechanism.

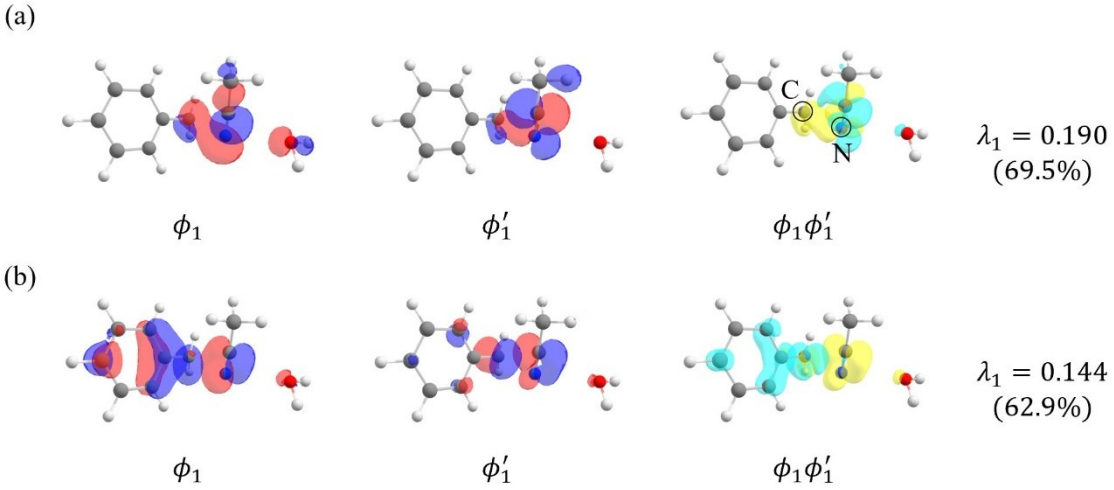

Figure 6. NRO results for the unsubstituted compound (X = H) at the branching region of the reaction path (s = 3.54 amu$^{1/2}$ bohr): (a) the occupied and virtual NROs (ϕ_1 and ϕ_1', respectively) along with their product ($\phi_1\phi_1'$) associated with structural changes along the IRC direction, and (b) those associated with structural changes along the branching direction.

C. NRO Analysis for the Fragmentation Reaction of the Substituted Compound (X = *p*-OMe)

As shown in Fig. 2, for electron-donating substituents X = *p*-NH_2 and *p*-OMe, the IRC leads to fragmentation instead of the Beckmann rearrangement. **Fig. 7** illustrates the structures of the reactant, TS, and product, and changes in energy and $\|\mathbf{\Lambda}\|_F^2$ along the IRC for the fragmentation reaction for X = *p*-OMe. The structures of R and TS are similar to those for X = H, but in P, fragmentation has occurred. Additionally, $\|\mathbf{\Lambda}\|_F^2$ shows peaks before the TS (s = −2.26 amu$^{1/2}$ bohr), near the TS (s = 0.24 amu$^{1/2}$ bohr), and after the TS (s = 13.4 and 22.6 amu$^{1/2}$ bohr). **Fig. 8** shows the NRO pairs and their products at each reaction coordinate. The NROs before the TS (a) and near the TS (b) are highly similar to those observed for X = H. Before the TS, intramolecular electron movement neutralizes the dissociating H_2O molecule (this is also seen in Fig. S1-2), while near the TS, electron movement from the C-C' σ orbital promotes the cleavage of the C-C' bond. In contrast, at s = 13.4 amu$^{1/2}$ bohr and s = 22.6 amu$^{1/2}$ bohr after the TS (Figs. 8c and 8d), CH_3CN has already dissociated, and fragmentation is progressing, with the NRO localized on the dissociated water molecule. In this region, bond formation and cleavage associated with the reaction are already complete, and it is intriguing to observe electron movement within the water molecule. As a characteristic of this system, the overall molecular charge is localized on the $MeOC_6H_4CH_2$ fragment. Under the electrostatic field generated by the cationic fragment, the rotation of the H_2O molecule, which has a dipole moment, induces intramolecular electron movement.

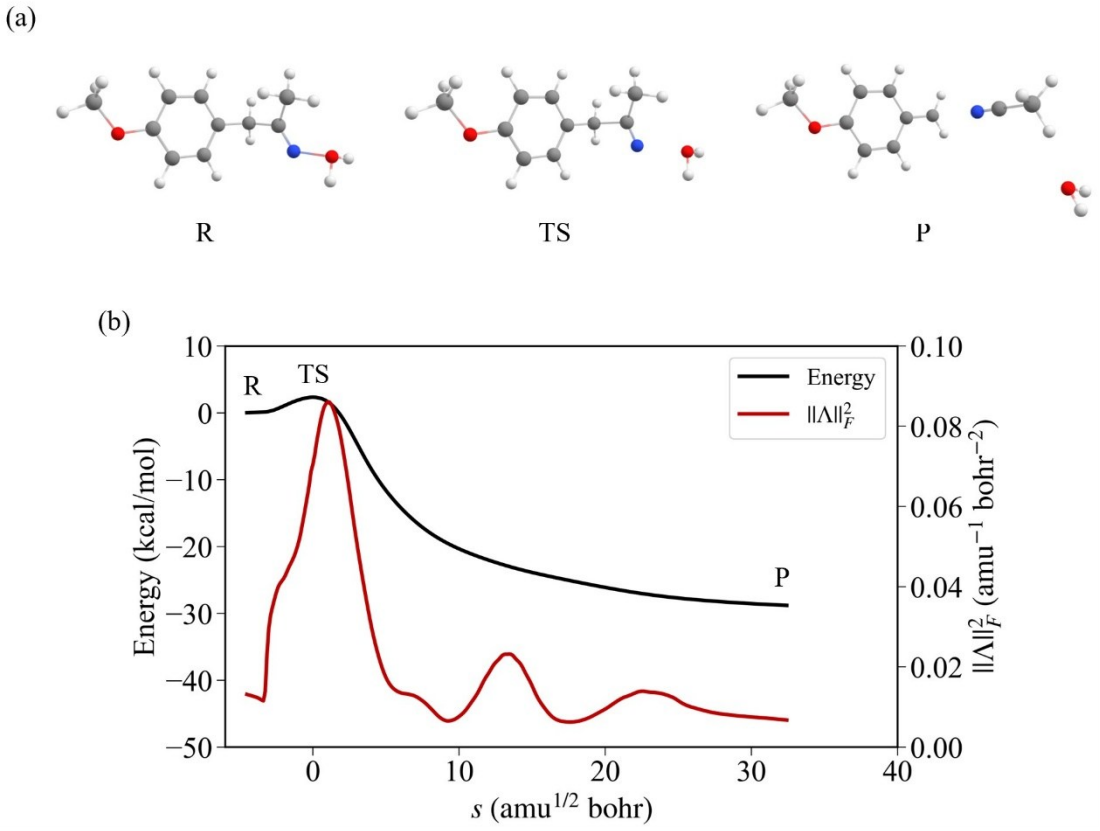

Figure 7. The fragmentation reaction for the substituted compound (X = *p*-OMe): (a) Structures of the reactant (R), TS, and product (P). (b) Changes in energy and $\|\boldsymbol{\Lambda}\|_F^2$ along the IRC.

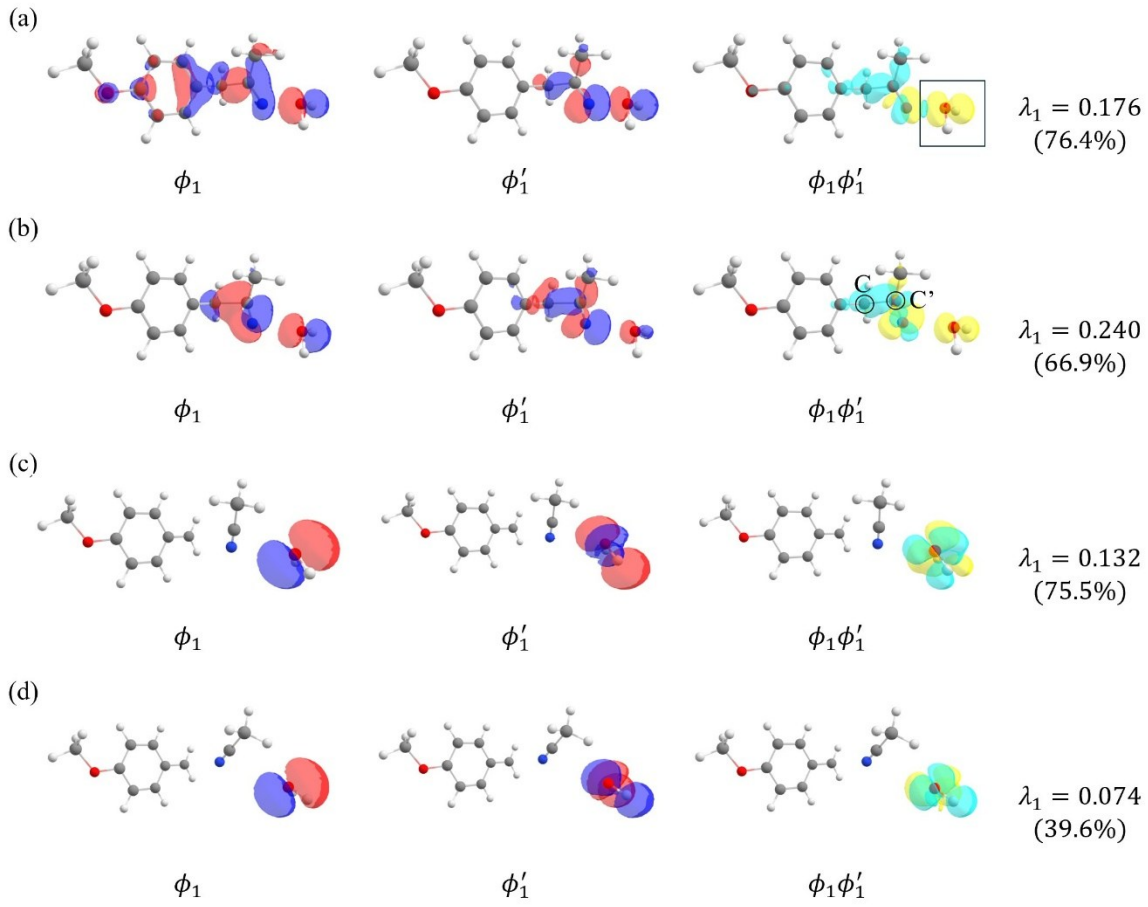

Figure 8. Occupied NRO (ϕ_1), virtual NRO (ϕ_1'), and their product ($\phi_1\phi_1'$) at the $\|\mathbf{\Lambda}\|_F^2$ peaks for the substituted compound (X = *p*-OMe): (a) $s = -2.26$ amu$^{1/2}$ bohr, (b) $s = 1.13$ amu$^{1/2}$ bohr, (c) $s = 13.4$ amu$^{1/2}$ bohr, and (d) $s = 22.6$ amu$^{1/2}$ bohr.

Next, vibrational analysis was performed along the IRC to investigate changes in the frequencies of projected vibrational modes. The results are shown in **Fig. 9a**. Although several imaginary frequency modes were observed, none of them corresponded to the molecular motion associated with the Beckmann rearrangement of interest. Focusing on the region near $s = 5$ amu$^{1/2}$ bohr (highlighted in red in Fig. 9a), where some vibrational

frequencies drop sharply, a mode related to the motion of the Beckmann rearrangement was identified (Fig. 9b). This mode is marked in blue for distinction in Fig. 9a. Although the frequency does not become imaginary, indicating no VRT, its sharp decline and its low frequency suggest that the curvature of the potential energy surface perpendicular to the IRC direction decreases and flattens in this region along the Beckmann rearrangement pathway. This implies that, given sufficient kinetic energy, the molecular system could proceed toward the Beckmann rearrangement product, and the direction of this mode can be considered as corresponding to the branching direction. At the structure where this mode's frequency reaches a minimum (s = 5.40 amu$^{1/2}$ bohr), NRO pairs were determined for structural changes along the IRC and branching directions to investigate electron movement behavior. **Fig. 10a** shows the NROs associated with structural changes along the IRC direction, while Fig. 10b shows those for the branching direction. For structural changes along the IRC, the electron moves from the benzene ring toward CH_3CN. Conversely, for structural changes along the branching direction, the electron moves from CH_3CN to the C-N σ orbital. Interestingly, compared to X = H, the roles of electron movement in the IRC and branching directions are reversed. This indicates that the behavior of electron movement is determined by which reaction pathway leads to either product.

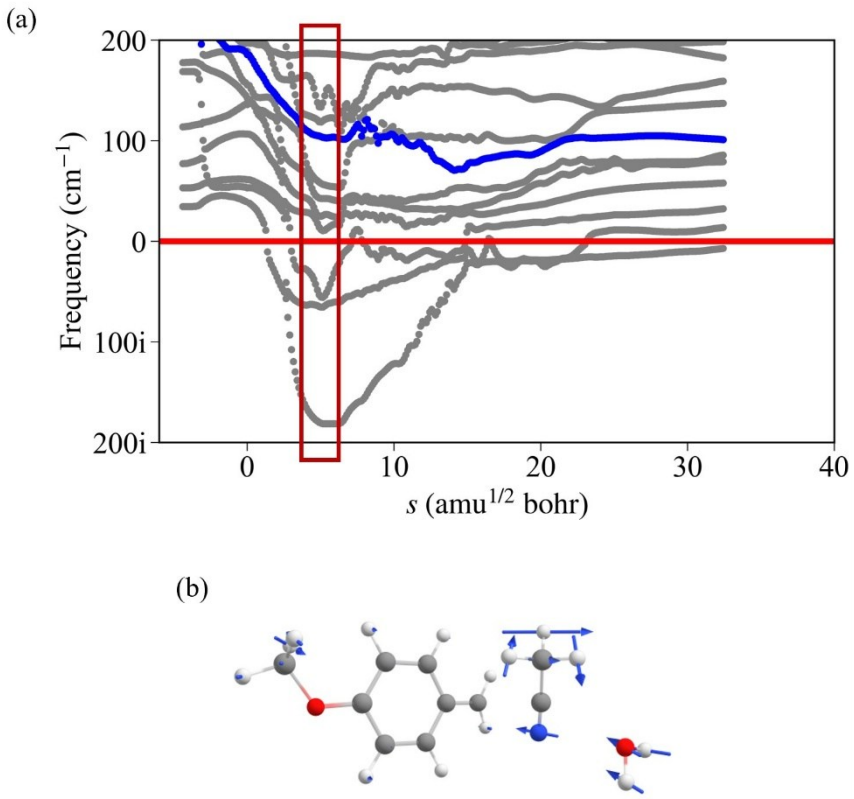

Figure 9. (a) Changes in the frequencies of projected vibrational modes along the IRC for the substituted compound (X = *p*-OMe), where the blue line represents the frequency of the vibrational mode associated with the Beckmann rearrangement. (b) The projected vibrational mode corresponding to the Beckmann rearrangement.

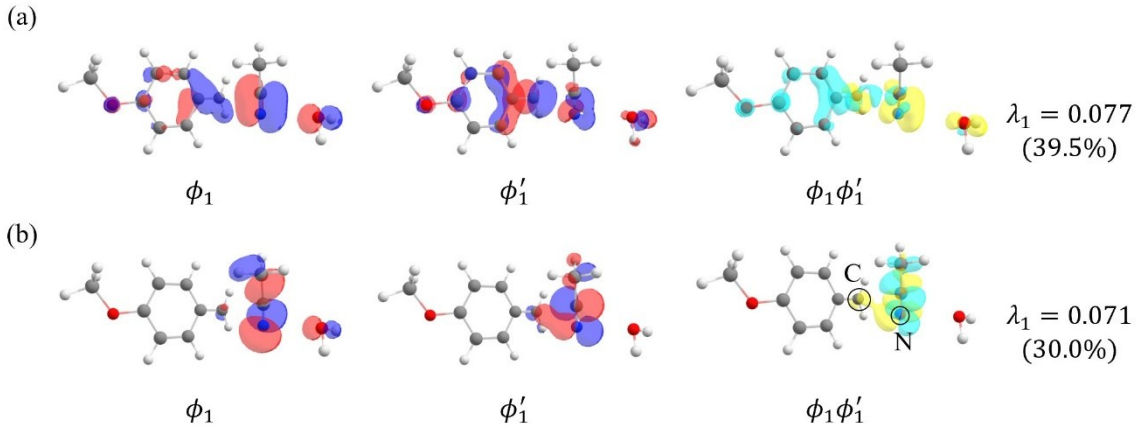

Figure 10. NRO results for the substituted compound (X = *p*-OMe) at the branching region of the reaction path (s = 5.40 amu$^{1/2}$bohr): (a) the occupied and virtual NROs (ϕ_1 and ϕ_1', respectively) along with their product ($\phi_1\phi_1'$) associated with structural changes along the IRC direction, and (b) those associated with structural changes along the branching direction.

D. Analysis of Substituent Effects

To gain deeper insights into substituent effects, we carried out NRO analysis at the reaction path bifurcation points for all substituents shown in Fig. 2 (See Fig. S3-1 to Fig. S4-8 in SI). Hereafter, we define the branching point as the structure where the magnitude of the imaginary frequency reaches a maximum (if VRT occurs), or where the frequency exhibits a minimum (if VRT does not occur), consistent with the approach used in Figs. 5 and 9. For example, the results for the electron-withdrawing substituent (X = *p*-NO_2) in Fig. S2 showed NROs almost identical to X = H, confirming that similar NRO results are obtained when the IRC behavior is consistent. Specifically, for all substituents, structural changes in the direction of the Beckmann rearrangement showed an increase in electron density in the C-N σ orbital, facilitating C-N bond formation. Conversely, structural changes in the fragmentation direction exhibited electron movement from the benzene ring to CH_3CN. Although Fig. S2 shows results for only three representative cases, it has been confirmed that the mode of electron movement is consistent across all ten substituents. This demonstrates the robustness of the observed electronic behaviors regardless of the substituent type.

To investigate the substituent effect influencing the termination of the IRC, we analyzed the "extent" of electron movement occurring in the branching region. Specifically, the extent of electron movement induced by orbital mixing within the NRO pair was evaluated using the singular value λ. NRO analysis was performed for both the IRC direction and the branching direction at the branching point for ten substituents, and the singular values corresponding to the rearrangement direction (λ_R) and the fragmentation direction (λ_F) were calculated. These results are summarized in **Table 1**. The analysis revealed that the relative

magnitudes of λ_R and λ_F determine the terminal structure of the IRC, except in the case of *p*-Me. This suggests that the singular values tend to reflect the preferred reaction pathway or the direction in which the reaction proceeds more favorably. In the *p*-Me case, the structure at the selected branching point differs significantly from those of the other substituents. Additionally, the formation of the C-N bond in *p*-Me occurs more slowly compared to the other cases that follow rearrangement pathways (Fig. 2), exhibiting behavior more similar to that of fragmentation reactions. These factors are believed to account for the deviation in the observed trend for *p*-Me compared to the other substituents. In addition, the ratio of λ_R to λ_F was calculated and plotted against a substituent parameter that accounts for electronic effects. The Hammett parameter σ [37] is commonly used to characterize substituent properties. However, because the substituents are adjacent to the benzene ring in this reaction, the resonance effects between the substituent and the benzene ring play a significant role in addition to their inherent electron-donating or electron-withdrawing properties. To account for these resonance effects, we used the parameter $\sigma^0 + r\Delta\bar{\sigma}_R^+$, derived from the Yukawa-Tsuno equation [38]. Here, *r* is a reaction-specific parameter indicating the resonance demand, and for the Beckmann rearrangement, a value of $r = 0.3$, as used by Yamataka *et al.* [24], was adopted. The substituent-specific constants σ^0 and $\bar{\sigma}_R^+$ were referenced from values provided in the literature [39]. **Figure 11** shows the plotted results of the ratio of singular values against $\sigma^0 + r\Delta\bar{\sigma}_R^+$. The ratio of singular values exhibits a high degree of linearity for $\sigma^0 + r\Delta\bar{\sigma}_R^+$. This result indicates that the relative magnitude of singular values effectively reflects the substituent effects.

From the above results, we identified a correlation between the relative magnitudes

of singular values and the electronic nature of substituents. This correlation suggests that substituents influence the extent of electron movement associated with either the rearrangement or fragmentation reaction, thereby determining the behavior of the IRC. For electron-donating substituents, the extent of electron movement associated with fragmentation is relatively greater, resulting in the IRC favoring the fragmentation pathway. This trend is reflected in the NRO pair product for the *p*-OMe case (Fig. 10a), which indicates significant electron movement originating from the oxygen atom in the substituent. The same trend is supported by the natural population analysis, which shows a sharp increase in the charge of the substituted benzyl cation after the TS (Fig. S1-2). In contrast, for electron-withdrawing substituents, electron movement associated with the rearrangement reaction is enhanced, making it easier for the reaction to proceed along the rearrangement pathway. This is consistent with the results of the natural population analysis, which show that the charge of substituted benzyl cation after the TS shifts from an increase to a decrease (Fig. S1-3). In conclusion, we found that the electronic nature of substituents modulates the extent of electron movement in the benzyl cation, thereby influencing the IRC pathway and the direction of bifurcation. This origin of the substituent effects is captured not only through the visualized NRO pairs, but also by examining the magnitudes of the singular values corresponding to reaction-involved directions.

Table 1. Summary of the NRO analysis and several parameters for ten substituents X. The $\sigma^0 + r\Delta\bar{\sigma}_R^+$ parameter, product type (R: Rearrangement or F: Fragmentation), singular values for rearrangement (λ_R) and fragmentation (λ_F) directions, and their ratio are shown.

X	$\sigma^0 + r\Delta\bar{\sigma}_R^+$	product	λ_R	λ_F	λ_R/λ_F
p-NH_2	-0.490	F	0.047	0.084	0.565
p-OMe	-0.310	F	0.071	0.077	0.925
m,m'-Me_2	-0.240	R	0.174	0.163	1.067
p-Me	-0.190	R	0.127	0.184	0.688
m-Me	-0.120	R	0.183	0.155	1.178
H	0	R	0.190	0.144	1.315
p-Cl	0.155	R	0.184	0.159	1.162
p-CHO	0.430	R	0.205	0.081	2.517
p-CN	0.730	R	0.210	0.078	2.698
p-NO_2	0.800	R	0.216	0.060	3.570

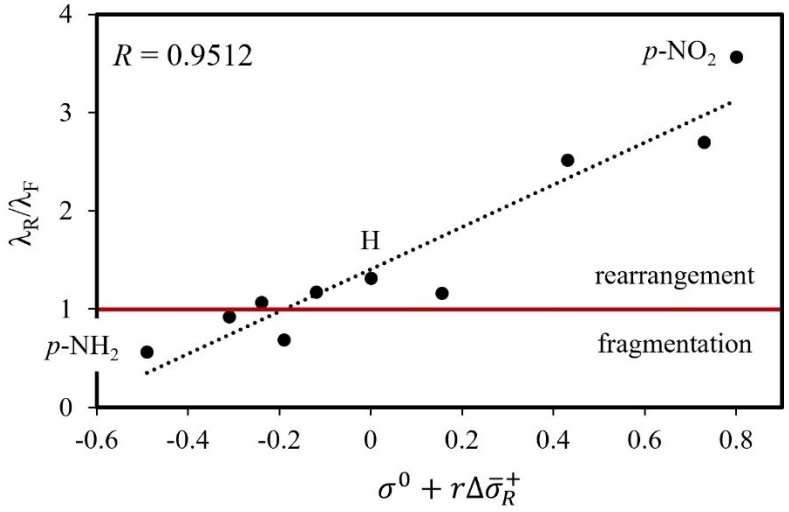

Figure 11. Ratio of singular values λ as a function of $\sigma^0 + r\Delta\bar{\sigma}_R^+$.

5. Conclusion

In this study, we investigated the Beckmann rearrangement of 1-phenyl-2-propanone oxime derivatives, which has been previously reported to exhibit reaction path bifurcation. We applied our recently developed NRO analysis to investigate electron movement behavior at the branching point of the reaction pathway along both the IRC direction and the branching direction. We first analyzed NROs along the IRC for X = H, leading to the rearrangement pathway, and X = *p*-OMe, leading to the fragmentation pathway. The results revealed similar electron movement behavior for both cases up to a certain point; however, in the rearrangement reaction, electron movement associated with C-N bond formation was observed, while in the fragmentation reaction, electron movement from the benzene ring toward CH_3CN was observed. Next, we identified branching points through vibrational frequency analysis of projected vibrational modes and compared NROs along the IRC and branching directions. The results in the cases of X = H and X = *p*-OMe revealed similar electron movement patterns for both substituents. Furthermore, a comprehensive discussion of substituent effects revealed a chemically reasonable correlation between the magnitude of singular values, the terminal product of the IRC, and substituent effects. This study establishes a quantitative framework for predicting and understanding reaction path bifurcation through systematic analysis of electron movement processes.

The significance of this study lies in its ability to discuss reaction path bifurcation from the perspective of electron movement. Traditionally, discussions of reaction path bifurcation have primarily relied on analyzing branching ratios examining the PES or through AIMD. While these approaches excel at capturing the influence of dynamics effects, which are the primary cause of reaction path bifurcations, they have largely overlooked the

perspective of electronic structures that underlie the PES governing molecular motion. The changes in electronic structures resulting from changes in these structures are deeply connected to reaction mechanisms. Therefore, the ability to examine reaction mechanisms in detail during reaction path bifurcation through this study represents a significant advancement. This will greatly enhance our understanding of the formation mechanisms of byproducts in chemical reactions.

Acknowledgments

The authors sincerely thank Dr. Shuichi Ebisawa, who developed the NRO method, for fruitful discussions on the current topic. This work was partly supported by JST, ACT-X Grant Number JPMJAX23DE, Japan, and JSPS KAKENHI grant number JP22K14640 to T. Tsutsumi, and by the Photo-excitonix Project in Hokkaido University, JST CREST grant number JPMJCR1902, and MEXT Program (Data Creation and Utilization-Type Material Research and Development Project Grant Number JPMXP1122712807) to T. Taketsugu. Part of the calculations were performed using the Research Center for Computational Science, Okazaki, Japan (Project: 22-IMS-C019).

Author Contributions

T. Nakanishi: Conceptualization, Methodology, Software, Investigation, Data curation, Writing – original draft, Writing – review & editing, Visualization.

T. Tsutsumi: Conceptualization, Methodology, Software, Writing – review & editing.

Y. Ono: Conceptualization, Methodology, Software, Writing – review & editing.

K. Sada: Writing – review & editing.

T. Taketsugu: Conceptualization, Methodology, Writing – original draft, Writing – review & editing, Resources, Funding acquisition.

Competing Interests

The authors declare no competing interests.

ORCID

Takuro Tsutsumi: 0000-0001-5086-112

Tetsuya Taketsugu: 0000-0002-1337-6694

References

[1] K. Fukui, *J. Phys. Chem.*, **74**, 4161 (1970).

[2] S. Maeda, Y. Harabuchi, Y. Ono, T. Taketsugu, and K. Morokuma, *Int. J. Quantum Chem.*, **115**, 258 (2015).

[3] H. Metiu, J. Ross, R. Silbey, and T. F. George, *J. Chem. Phys.*, **61**, 3200 (1974).

[4] P. Valtazanos and K. Ruedenberg, *Theor. Chim. Acta*, **69**, 281 (1986).

[5] W. Quapp, *Theor. Chim. Acta*, **75**, 447 (1989).

[6] T. Taketsugu, N. Tajima, and K. Hirao, *J. Chem. Phys.*, **105**, 1933 (1996).

[7] T. Yanai, T. Taketsugu, and K. Hirao, *J. Chem. Phys.*, **107**, 1137 (1997).

[8] T. Taketsugu and T. Hirano, *J. Chem. Phys.*, **99**, 9806 (1993).

[9] W. H. Miller, N. C. Handy, J. E. Adams, *J. Chem. Phys.*, **72**, 99 (1980).

[10] J. M. Bofill, W. Quapp, *J. Math. Chem.*, **51**, 1099 (2013).

[11] S. Shaik, D. Danovich, G. N. Sastry, P. Y. Ayala, and H. B. Schlegel, *J. Am. Chem. Soc.*, **119**, 9237 (1997).

[12] Y. Harabuchi and T. Taketsugu, *Theo. Chem. Acc.*, **130**, 305 (2011).

[13] Y. J. Hong and D. J. Tantillo, *Nature Chemistry*, **6**, 104 (2014).

[14] P. Yu, T. Q. Chen, Z. Yang, C. Q. He., A. Patel, Y. Lam, C. Liu, and K. N. Houk, *J. Am. Chem. Soc.*, **139**, 8251 (2017).

[15] T. Murakami, D. Hayashi, Y. Kikuma, K. Yamaki, and T. Takayanagi, *J. Comput. Chem.*, **45**, 2778 (2024).

[16] K. Fukui, T. Yonezawa, and H. Shingu, *J. Chem. Phys.*, **20**, 722 (1952).

[17] S. Maeda, K. Ohno, and K. Morokuma, *Phys. Chem. Chem. Phys.*, **15**, 3683 (2013).

[18] T. Tsuneda and R. K. Singh, *J. Comput. Chem.*, **35**, 1093 (2014).

[19] T. Tsuneda, H. Sumitomo, M. Hasebe, T. Tsutsumi, and T. Taketsugu, *J. Comput. Chem.*, **44**, 93 (2022).

[20] M. Hasebe, T. Tsutsumi, T. Taketsugu, and T. Tsuneda, *J. Chem. Theory Comput.*, **17**, 6901 (2021).

[21] S. Ebisawa, M. Hasebe, T. Tsutsumi, T. Tsuneda, and T. Taketsugu, *Phys. Chem. Chem. Phys*., **24**, 3532 (2022).

[22] S. Ebisawa, T. Tsutsumi, and T. Taketsugu, *J. Chem. Phys*., **157**, 084118 (2022).

[23] H. Yamataka, M. Sato, H. Hasegawa, and S. C. Ammal, *Faraday Discuss*., **145**, 327 (2010).

[24] M. Sato and H. Yamataka, *J. Synth. Org. Chem. Jpn*., **72**, 393 (2014).

[25] G. Knizia, *J. Chem. Theory Comput.*, **9**, 4834 (2013).
[26] G. Knizia and J. E. M. N. Klein, *Angew. Chem. Int. Ed.*, **54**, 5518 (2015).
[27] R. McWeeny, *Rev. Mod. Phys.*, **32**, 335 (1960).
[28] J. Gerratt, and I. M. Mills., *J. Chem. Phys.*, **49**, 1719 (1968).
[29] J. A. Pople, R. Krishnan, H. B. Schlegel, and J. S. Binkley, *Int. J. Quantum Chem.*, **13**, 225 (1979).
[30] M. Frisch, *Chem. Phys.*, **141**, 189 (1990).
[31] A. Morita and S. Kato, *J. Am. Chem. Soc.*, **119**. 4021 (1997).
[32] M. Miyamoto and M. Hada, *J. Comput. Chem.*, **41**, 1628 (2020).
[33] K. Yamaguchi and Y. Yamakita, *Chem. Phys. Lett.*, **849**, 141444 (2024).
[34] R. L. Matrin, *J. Chem. Phys.*, **118**, 4775 (2003).
[35] M. J. Frisch, G. W. Trucks, H. B. Schlegel, G. E. Scuseria, M. A. Robb, J. R. Cheeseman, G. Scalmani, V. Barone, G. A. Petersson, H. Nakatsuji, X. Li, M. Caricato, A. V. Marenich, J. Bloino, B. G. Janesko, R. Gomperts, B. Mennucci, H. P. Hratchian, J. V. Ortiz, A. F. Izmaylov, J. L. Sonnenberg, D. Williams-Young, F. Ding, F. Lipparini, F. Egidi, J. Goings, B. Peng, A. Petrone, T. Henderson, D. Ranasinghe, V. G. Zakrzewski, J. Gao, N. Rega, G. Zheng, W. Liang, M. Hada, M. Ehara, K. Toyota, R. Fukuda, J. Hasegawa, M. Ishida, T. Nakajima, Y. Honda, O. Kitao, H. Nakai, T. Vreven, K. Throssell, J. A. Montgomery, Jr, J. E. Peralta, F. Ogliaro, M. J. Bearpark, J. J. Heyd, E. N. Brothers, K. N. Kudin, V. N. Staroverov, T. A. Keith, R. Kobayashi, J. Normand, K. Raghavachari, A. P. Rendell, J. C. Burant, S. S. Iyengar, J. Tomasi, M. Cossi, J. M. Millam, M. Klene, C. Adamo, R. Cammi, J. W. Ochterski, R. L. Martin, K. Morokuma, O. Farkas, J. B. Foresman and D. J. Fox, Gaussian 16 (Revision C.01), Gaussian Inc., Wallingford, CT, 2016.
[36] A. E. Reed, R. B. Weinstock, and F. Weinhold, *J. Chem. Phys.*, **83**, 735 (1985).
[37] L. P. Hammett, *J. Am. Chem. Soc.*, **59**, 96 (1937).
[38] Y. Yukawa, Y. Tsuno, *Bull. Chem. Soc. Jpn.*, **32**, 971 (1959).
[39] M. Mishima, Mustanir, M. Fujio, and Y. Tsuno, *Bull. Chem. Soc. Jpn.*, **69**, 2009 (1996).